Supporting Information for:

An Endogenous dAMP ligand in *Bacillus subtilis* class Ib RNR promotes assembly of a noncanonical dimer for regulation by dATP

Mackenzie J. Parker[a], Ailiena O. Maggiolo[b,1], William C. Thomas[c,1], Albert Kim[a], Steve P. Meisburger[c], Nozomi Ando[c,2], Amie K. Boal[b,d,2], and JoAnne Stubbe[a,e,2]

[a]Department of Chemistry and [e]Department of Biology, Massachusetts Institute of Technology, Cambridge, MA 02139; [b]Department of Biochemistry and Molecular Biology and [d]Department of Chemistry, The Pennsylvania State University, University Park, PA 16802; [c]Department of Chemistry, Princeton University, Princeton, NJ 08544

[1]Each author contributed equally and the order is alphabetical.

[2]To whom correspondence should be addressed: Email: nozomi.ando@princeton.edu, akb20@psu.edu, stubbe@mit.edu

Corresponding author: JoAnne Stubbe, 77 Massachusetts Ave., Room 18-581, Cambridge, MA 02139, stubbe@mit.edu, (617) 253-1814

Major classification: Biological Sciences, *Minor classification:* Biochemistry

Keywords: nucleotide metabolism, allostery, protein structure, partial ATP-cone

Short title: dATP inhibition in a Ib ribonucleotide reductase

Supporting Methods

Materials. Chemicals were purchased at the highest purity available. Nucleotides were purchased from Sigma-Aldrich or MP Biomedicals and were used as received. Plastic-backed polyethyleneimine (PEI) – cellulose TLC plates impregnated with short- and long-wave UV fluorescent compounds were from Sigma. Non-fluorescent PEI-cellulose plates were from Macherey-Nagel. Chemically competent *E. coli* BL21 (DE3) and BL21 (DE3) Codon Plus RPIL cells were from Agilent. Primers were purchased from Invitrogen. Phusion® High Fidelity DNA polymerase and restriction enzymes were from New England Biolabs. DL-dithiothreitol (DTT) and T4 DNA ligase were from Promega. The vector pTB145, encoding His_6-tagged SUMO protease, was a gift from Dr. Bradley Pentelute (Department of Chemistry, MIT). It was transformed into BL21 (DE3) Codon Plus RPIL cells and the protein overexpressed and purified as described previously (1)**.**

Cloning the *B. subtilis* RNR genes into pE-SUMO. All cloning used the touchdown PCR method (2). *nrdE* and *nrdI* were amplified from *B. subtilis* JH624 genomic DNA using the primers listed in **Table S4** to introduce 5′ *BsaI* and 3′ *SacI* (*nrdE*) or *XhoI* (*nrdI*) restriction sites. The amplicons were digested and ligated into similarly treated pE-SUMO (LifeSensors, Kan^r) using T4 DNA ligase. *nrdF* has an internal *BsaI* restriction site and was cloned in two steps. In the first step, the last 375 bp of *nrdF* was amplified using Primer#1 and Primer#2 (**Table S4**) to introduce 5′ *SacI* and 3′ *XhoI* restriction sites. The digested amplicon was ligated into pE-SUMO to generate the vector pE-SUMO-$nrdF_{Cterm}$. In the second step, the first 631 bp of *nrdF* was amplified using Primer#3 and Primer#4 (**Table S4**) to introduce *BsaI* sites at the 5′ and 3′ ends of the amplicon. The primers were designed such that mutually exclusive sticky ends were generated at the amplicon ends so that it could be ligated into pE-SUMO-$nrdF_{Cterm}$ in only one orientation. The

resulting amplicon was digested with BsaI and ligated into similarly digested pE-SUMO-*nrdF*$_{Cterm}$, thus generating an intact copy of *nrdF* in pE-SUMO. Sequencing of the vectors (MIT Biopolymers Laboratory) confirmed the successful cloning of all three genes. Site-directed mutagenesis was performed using the Phusion® High-Fidelity DNA Polymerase (New England BioLabs) PCR protocol and the primers listed in **Table S4** to generate pE-SUMO-*nrdE*-$H_{34}Q$ and $F_{37}I$, which were verified by sequencing (Quintara Biosciences).

Expression and purification of tagless *B. subtilis* RNR proteins. The vectors pE-SUMO-*nrdE*, -*nrdF*, and -*nrdI* were transformed into BL21 (DE3) cells and the His_6-Smt3-tagged proteins were overproduced as described previously (3-5). Typical yields (in g cell paste L^{-1}) were 2.8, 1.7, and 2.6 for His_6-Smt3-NrdE, -NrdF, and -NrdI. His_6-Smt3-NrdE and -NrdF were purified as described previously (3-5). The purification of His_6-Smt3-NrdI was the same as previously described up through the Ni-NTA affinity step (5). Appropriate fractions were pooled, diluted 5-fold with 50 mM Tris, pH 8.5, 5% (w/v) glycerol (Tris buffer) plus 100 mM NaCl, and loaded onto a Q-Sepharose column (5.7 x 2.5 cm, ~28 mL) equilibrated in diluent. The column was washed with 2 CVs of diluent before eluting His_6-Smt3-NrdI (~230 mM NaCl) using a 300 mL linear gradient from 100 – 500 mM NaCl in Tris buffer. Protein-containing fractions were pooled and stored at -80 °C. Concentrations of His_6-Smt3-NrdE and His_6-Smt3-NrdF were determined using ε_{280} = 80600 and 56300 M^{-1} cm^{-1}, respectively, while the concentration of His_6-Smt3-NrdI was determined using the bicinchoninic acid assay (Pierce) with BSA as a standard (6, 7).

All steps for the removal of the His_6-Smt3 tag and subsequent purification of the tagless proteins were conducted at 4 °C. The His_6-Smt3 tag was cleaved from NrdE and NrdF typically at 150 μM using a 500:1 mole ratio of tagged protein:SUMO protease. His_6-Smt3-NrdF was supplemented with DTT to 5 mM prior to the addition of SUMO protease. The samples were then

incubated for 2 h and either stored at -80 °C or loaded directly onto a Ni-NTA column (4.0 x 1.5 cm, 7 mL) equilibrated in 50 mM sodium phosphate, pH 7.6, 150 mM NaCl, 5% (w/v) glycerol, and either 40 mM imidazole and 10 mM BME (NrdE) or 20 mM imidazole (NrdF). The column was washed with 9 CVs of equilibration buffer and 20 x 3 mL fractions were collected. Protein-containing fractions were pooled, concentrated, and exchanged into storage buffer on a Sephadex G25 column (28 x 1.5 cm, ~49 mL): NrdE into 50 mM sodium phosphate, pH 7.6, 150 mM NaCl, 5% (w/v) glycerol, 10 mM DTT; and NrdF into 50 mM HEPES, pH 7.6, 5% (w/v) glycerol. Yields (>97% pure by SDS-PAGE) relative to the starting amounts of His_6-Smt3-tagged protein were 90% NrdE and 89% NrdF. Protein concentrations were estimated using ε_{280} = 79100 M^{-1} cm^{-1} and 54800 M^{-1} cm^{-1} for NrdE and NrdF, respectively.

Tag removal from His_6-Smt3-NrdI used 1.2 mL of ~550 μM protein supplemented with 5 mM DTT and 20 μM SUMO protease (mole ratio ≈ 25:1). The reaction was incubated for 24 – 48 h at 4 °C and either stored at -80 °C or directly loaded onto a Ni-NTA column (4.0 x 1.5 cm, 7 mL) in 50 mM sodium phosphate, pH 7.6, 150 mM NaCl, 20 mM imidazole, 5% (w/v) glycerol. The column was washed with 7 CVs buffer and 20 x 2.5 mL fractions were collected, with tagless NrdI eluting in fractions 1 – 5. These fractions were pooled and placed in a 50-mL beaker to which was added 10 mg FMN (Sigma Aldrich, purity 73 – 79%) and 50 mM sodium phosphate (pH 7.6) buffer to give final concentrations of 50 mM sodium phosphate, pH 7.6, 94 mM NaCl, 12.5 mM imidazole, 3% (w/v) glycerol, 1 mM FMN, and ~35 μM NrdI in 20 mL. The beaker was wrapped in foil and the contents stirred at 4 °C for 4 – 6 h. The solution was then concentrated to ~1.5 mL using a pressurized Amicon stirred cell with a 10000 MWCO regenerated cellulose membrane. The sample was then buffer exchanged on a Sephadex G25 column (28 x 1.5 cm, 49 mL) into 50 mM HEPES, pH 7.6, 5% (w/v) glycerol. Protein-containing fractions were pooled and

concentrated to ~1 mL to give 500 – 600 μM NrdI in 84 % yield and > 97% purity. The FMN load and ε_{449} (11900 M^{-1} cm^{-1}) of NrdI was assessed by the method of Mayhew and Massey (8). To assess the FMN load, the protein pellet was dissolved in 200 μL Edelhoch buffer (6 M guanidinium HCl, 20 mM sodium phosphate, pH 6.5) and the amount of protein quantitated by A_{280} (ε_{280} = 9530 M^{-1} cm^{-1}, calculated as described by Gill and von Hippel) (9, 10).

Separation of apo- and holo-NrdE by MonoQ anion exchange chromatography. As-isolated NrdE (aiNrdE, 35 nmol, 1 mL, ~ 0.7 dAXP/α (X = M, D, T)) in storage buffer (50 mM sodium phosphate, pH 7.6, 150 mM NaCl, 5% (w/v) glycerol, 10 mM DTT) was centrifuged (20000 x g, 4 min, 4 ºC) and loaded onto a MonoQ 10/100 GL column (8 mL) connected to a BioCAD Sprint FPLC system (PerSeptive Biosystems) and equilibrated in Tris buffer (50 mM Tris, pH 7.6, 5% (w/v) glycerol, 1 mM tris(2-carboxyethyl)phosphine (TCEP)) supplemented with 100 mM NaCl. The column was washed with 10 mL of equilibration buffer and the protein eluted with a 160 mL linear gradient from 100 – 500 mM NaCl in Tris buffer at a flow rate of 1 mL min^{-1}. Apo-NrdE eluted between 260 – 270 mM NaCl and holo-NrdE between 330 – 350 mM NaCl (**Fig. S3A**). Protein fractions in each region were pooled, concentrated, and stored at -80 °C. At a later date, multiple isolates of either apo- or holo-NrdE obtained through the procedure described above were pooled and rechromatographed on the MonoQ column to generate a homogenous preparation of the desired protein (**Fig. S3B** and **C**). These samples were exchanged into storage buffer by gel filtration on a Sephadex G25 column and assayed for dAXP as described below.

Spectrophotometric assays. Assays monitoring NADPH consumption (ε_{340} = 6220 M^{-1} cm^{-1}) were conducted at 37 ºC using a Varian Cary 3 spectrophotometer and contained in a volume of 500 μL: 50 mM HEPES, pH 7.6, 15 mM $MgCl_2$, 1 mM EDTA, 40 μM TrxA, 0.4 μM TrxB, 0.2 mM NADPH, 0.5 μM Mn-β_2 (0.9 Y•/β_2), and 0.5 μM NrdE. Assays assessing substrate specificity

allosteric regulation were carried out with aiNrdE (0.7 ± 0.1 dAXP/α (X = M, D, T), see **Fig. 2** and **Table S1**). Assays to determine the effect of dATP on activity were carried out with either apo-NrdE (≤ 0.02 dAXP/α) or holo-NrdE (1.1 ± 0.2 dAMP/α). All assay solutions were incubated at 37 ºC for 2 min prior to adding either β_2 or substrate to initiate turnover. To measure steady-state kinetic parameters for effectors, substrate concentrations were held at 1 mM while effector concentrations varied: ATP (25 μM – 4 mM), dGTP (250 nM – 4 mM), TTP (100 nM – 4 mM). To measure steady-state parameters for substrates, the appropriate effector was present ~10x its K_m^{app} (**Table S2**), while the substrate concentration was varied: ADP (25 μM – 8 mM), CDP (10 μM – 2 mM), GDP (10 μM – 1 mM), UDP (25 μM – 4 mM). Data were fit to the Michaelis-Menten and Hill equations using non-linear regression in Igor Pro (Wavemetrics, Lake Oswego, OR). The statistical significance of better fits to the Hill equation were assessed using an extra sum-of-squares F test with a threshold $p = 0.01$. To assess the inhibitory properties of dATP on UDP reduction catalyzed by aiNrdE and CDP reduction catalyzed by apo- and holo-NrdE, the substrate concentration was 1 mM and dATP concentrations spanned 250 nM to 1 mM.

SV-AUC analysis of aiNrdE with nucleotides. SV-AUC was performed using a Beckman XL-1 analytical ultracentrifuge with interference optical detection at the MIT Biophysical Instrumentation Facility essentially as described previously (4). Cells assembled with Epon charcoal double sector centerpieces and sapphire windows were loaded with ~440 μL samples of 1.0 – 1.2 μM aiNrdE with dATP (0.5 – 100 μM) or TTP (0.12 μM – 12 μM) prepared in AUC buffer (50 mM HEPES, pH 7.6, 150 mM NaCl, 15 mM $MgCl_2$, and 1 mM TCEP). The experiments were performed at 20 °C and an angular velocity of 42000 rpm. For samples with 0-50 μM dATP or 0.12 – 12 μM TTP, the first 250 scans of each data set were time stamp corrected (11) and then fit to the c(s) model augmented with the buffer sedimentation correction module (12) in the

program Sedfit (13, 14). The resulting $s_{20,w}$ distributions were corrected to standard state using a buffer density = 1.009 g mL^{-1}, buffer viscosity = 1.054 cP, and partial specific volume = 0.7324 cm^3 g^{-1} for NrdE, which were calculated with the program Sednterp (15). The program HYDROPRO (16) was used to predict the $s_{20,w}$ for the NrdE monomer and dimer as described previously (4).

The SV-AUC data for the sedimentation of 1.0 μM aiNrdE in the presence of 100 μM dATP was different from those produced at lower dATP concentrations in that two distinct sedimentation boundaries were observed. One boundary corresponded to large species of NrdE that completed sedimentation within the first 10 – 15 scans of the experiment and that could not be satisfactorily fit with any of the models of Sedfit. Analysis of these scans was therefore performed with the program DCDT+ developed by John Philo (version 2.4.3) (17, 18), which does not attempt to deconvolute the diffusion coefficients of sedimenting species. The apparent sedimentation coefficient distribution, g(s*), resulting from this analysis displays an upturn at low $s_{20,w}$ values and a broad peak spanning ~60-130 S. Assuming that NrdE produces a shift of 3.3 fringes per 1 mg mL^{-1}, approximately 30% of the protein is accounted for in the broad peak as large dATP-induced oligomers/aggregates. To learn more about the smaller species present at 100 μM dATP, we fit scans 16 – 200 using the c(s) model in Sedfit as described above. The resulting c(s) distribution (**Fig. S2A**, bottom curve) revealed the same two-peak structure observed at lower dATP concentrations, albeit with slight higher sedimentation coefficients (6.8 S and 9.3 S).

Quantitation of dAMP bound to NrdE. Prior to quantitation of nucleotide, DTT, glycerol, and Tris buffer, which contribute to absorption features in the UV, were removed by exchanging aliquots of NrdE into 50 mM sodium phosphate, pH 7.6, 150 mM NaCl using three to four rounds of dilution-concentration with Amicon Ultra-0.5 YM30 microcentrifugal filters (EMD

Millipore). Replicate samples of NrdE (~45 μM, ~100 μL) were then immersed in a boiling water bath for 10 min and cooled on ice. The precipitated protein was pelleted by centrifugation (21130 x g, 10 min, 4 ºC) and the supernatant was transferred to a new container. The pellet was centrifuged again and any remaining liquid was pipetted off and combined with the supernatant from the first spin. The total volume of the supernatant was determined and its A_{260} (ε_{260} = 15400 M^{-1} cm^{-1}) was measured. The protein pellet was dissolved in 200 μL Edelhoch buffer (6 M guanidinium HCl, 20 mM sodium phosphate, pH 6.5) and the amount of protein quantitated by A_{280} (ε_{280} = 70830 M^{-1} cm^{-1}, calculated as described by Gill and von Hippel) (9, 10).

Alternatively, aiNrdE or endogenous NrdEF were exchanged via Sephadex G50 into 50 mM Tris pH 7.6, 30 mM NaCl to remove glycerol and DTT and then precipitated by addition of $HClO_4$ to a final concentration of 1%. The precipitated protein was removed by centrifugation, and the supernatant was neutralized with ice cold 2M KOH at 4°C. After 1 h at -20°C, the $KClO_4$ was removed by centrifugation and the A_{260} was measured as described above. Control experiments indicated that neither denaturation procedure hydrolyzed dATP.

Nucleotide isolation and identification: PEI-cellulose TLC and ^{1}H-NMR. To identify the nucleotide(s) bound to aiNrdE, a total of 4 protein preparations were denatured using the methods described in the previous section. For two isolates (1.4 μmol dAXP total), the protein was dialyzed against 3 x 4L of water over 8h at 4°C prior to heat denaturation. The other preparations were precipitated with $HClO_4$ following buffer exchange and worked up as described above.

a. PEI-cellulose TLC. Solutions of (d)AMP, (d)ADP, and (d)ATP for nucleotide standards were prepared in 1.8 mM Tris, pH 7.5. For fluorescent (non-fluorescent) plates, the origin was spotted with 9 – 20 nmol (50 – 300 pmol) of nucleotide standards and unknown. Three development solvents were used: (1) 1.5 M LiCl (which separates all 3 phosphorylation states),

(2) 0.5 M formic acid pH 3.4 (which resolves mono and diphosphates), and (3) a 3:1 mixture of 4 M formic acid (pH 3.4):4% (w/v) boric acid (which resolves di and triphosphates) (19, 20). The nucleotides were detected using the Hanes/Isherwood spray for inorganic phosphate (20) or short wavelength UV light for fluorescent plates.

b. ^{1}H-NMR. The supernatant recovered from the heat denaturation method (1.4 μmol) was diluted to 10 mL with water and loaded onto a DEAE Sephadex A-25 column (3.5 x 0.8 cm, 1.8 mL). The column was washed with additional water and the nucleotides were eluted together using 7 mL of 500 mM NH_4HCO_3 (pH 7.8). All the eluent was pooled and the NH_4HCO_3 was removed by repeated rounds of lyophilization/dissolution to give 1.1 μmol (A_{260}). From this material 0.75 μmol was loaded onto a second DEAE Sephadex A-25 column (9 x 1 cm, 7 mL) equilibrated in 50 mM TEAB, pH 7.5. The column was washed with 7 CVs of 50 mM TEAB and the nucleotides were eluted with a 75 x 75 mL linear gradient from 50 – 400 mM TEAB, pH 7.5, followed by a 30 x 30 mL linear gradient of 400 – 600 mM TEAB. Fractions were screened for A_{260} and material eluted at 230 mM (monophosphate), 390 mM (diphosphate), and 550 mM (triphosphate) TEAB. Appropriate fractions were pooled and the TEAB removed by repeated lyophilization/dissolution. The ratio of the recovered material was 55%: 32%: 12% of the mono-, di-, and triphosphates. Alternatively, the supernatant from the tagless NrdE (600 mg) pelleted with $HClO_4$ was neutralized and the $KClO_4$ removed. The supernatant was then directly analyzed by DEAE-Sephadex A25 as described above. Only monophosphorylated nucleotide (0.75 equiv) was recovered using this denaturation procedure and NMR analysis identified it as dAMP.

^{1}H-NMR spectra of the recovered mono-, di-, and triphosphates exchanged into D_2O were acquired on a Varian Inova-500 MHz spectrometer in the MIT Department of Chemistry Instrumentation Facility. The material in the monophosphate region had chemical shifts and

coupling constants consistent with an authentic sample of dAMP: *H2* = 8.07 ppm (s, 1H); *H8* = 8.30 ppm (s, 1H); *H1′* = 6.35 ppm (t, 1H); *H2′(pro*-R*)* = 2.41 ppm (m, 1H); *H2′(pro*-S*)* = 2.64 ppm (m, 1H); *H3′* = 4.54 ppm (m, 1H); *H4′* = 4.10 ppm (m, 1H); *H5′* = 3.86 ppm (m, 2H); $J_{H1',H2'(pro\text{-}R)}$ = 6.5 Hz; $J_{H1',H2'(pro\text{-}S)}$ = 7.0 Hz, $J_{H2'(pro\text{-}S),H2'(pro\text{-}R)}$ = 14 Hz. The small differences in chemical shifts are due to differences in salt and nucleotide concentrations and small pH changes between the sample and standards. The material eluting from the DEAE A25 column in the di- and triphosphate regions could not be definitively identified but exhibited several downfield chemical shifts indicative of a purine nucleobase and anomeric C1′ protons (1).

Identification and quantitation of dAMP bound to *Bs*NrdEF. *a. Isolation. Bs*NrdEF in 50 mM Tris, pH 7.6, 30 mM NaCl (200 µL, 14.4 µM $\alpha_2\beta_2$ assuming a 1:1 subunit ratio and ε_{280} = 267800 M^{-1} cm^{-1}) was precipitated at 4 °C with 1% $HClO_4$, incubated for 10 min, and centrifuged (21,000 x g, 10 min, 4 °C). The supernatant was neutralized with ice-cold 2 M KOH (18 µL) prior to being frozen in liq. N_2, thawed, and clarified by centrifugation (21,000 x g). The amount of dAMP recovered in the supernatant was quantitated by UV-visible spectroscopy. dAMP standards (0.5, 1, 5, 10 µM) were prepared in 50 mM Tris pH 7.6 and treated with $HClO_4$ as described above.

b. Mass spectrometric identification and quantitation. LC-MS and MS/MS analysis for nucleotide identification and quantitation was performed using a Thermo q-Exactive Plus mass spectrometer coupled to a Thermo Ultimate 3000 HPLC. Electrospray source settings: sheath gas flow rate = 35 L min^{-1}, auxiliary gas flow rate = 5 L min^{-1}, capillary temperature = 250 °C, auxiliary gas temperature =300 °C. The desired m/z range was calibrated using a Thermo LC-MS Calibration mix immediately before the analysis. A scan range of 66.7-1000 m/z was used at a resolving power of 70,000 with alternating positive and negative ion mode scans. Samples were injected onto on a SeQuant ® ZIC®-pHILIC column (EMD Millipore, 5 µm, PEEK, 100 mm x

2.1 mm) at a flow rate of 0.1 mL min^{-1}. Mobile phase A was 20 mM NH_4HCO_3 with 0.1% NH_4OH, and mobile phase B was acetonitrile. The mobile phase composition started at 100 % B, and decreased to 40 % B over 20 min. The column was then washed with 0 % B for 5 min before re-equilibration to 100 % B over 15 min. The extracted ion currents were plotted using a mass accuracy window of 5 ppm around the predicted monoisotopic *m/z* value of the molecular ion of each metabolite of interest (dAMP, dADP, dATP, GDP, and GTP). The integrated area of each peak was provided to give the response to the standard dAMP samples that were injected onto the system in random order. Two blank runs were run after each standard and prior to the analysis of the sample of interest. A linear fit to the standard curve was used to calculate concentrations for the endogenous samples. For high resolution MS the same spectrometer and 10 cm column with a 3 mm guard column were used. The column was calibrated before use with Pierce Negative Ion Calibration mix (Prod Number 88324). The monoisotopic *m/z* was 331.0609 for the dAMP standard and the as-isolated unknowns. Fragmentation analysis of ions by MS/MS in the Orbitrap (FT) mass analyzer produced mass accuracies of < 5 ppm. Fragment *m*/*z* $[M+H]^+$ for dAMP standard and *Bs*NrdEF-derived nucleotide: 78.959, 96.970, 134.047, 176.996, 195.007, 330.062.

X-ray crystallographic characterization of *B. subtilis* NrdE. *a. General crystallographic methods.* All crystallographic datasets were collected at either the Life Sciences Collaborative Access Team (LS-CAT) or the National Institute of General Medical Sciences and National Cancer Institute Collaborative Access Team (GM/CA-CAT) beamlines at the Advanced Photon Source (Argonne National Laboratory) or the Macromolecular Crystallography beamline at the Advanced Light Source (Berkeley National Laboratory). Diffraction images were processed using the HKL2000 software package (21) and resolution limits were determined by evaluation of the Pearson correlation coefficient, $CC_{1/2}$ (22). Initial structures were solved using the online

molecular replacement server BALBES (23), which identified the coordinates of NrdE from *Salmonella typhimurium* (PDB accession code 1PEM) (24) as the initial search model. REFMAC5 (25), implemented within CCP4 (26), and Coot (27) were used for model building and refinement. All structures were validated and analyzed for Ramachandran parameters with the Molprobity server (28). All data collection and model refinement statistics are listed in **Table S3**. Electron density maps were calculated using the FFT program (29) and electrostatic surface potential maps were generated with the APBS plugin in PyMOL. Figures were generated using PyMol molecular graphic systems (Schrödinger, LLC) and the CONSURF server (30). Ligand interaction maps were generated using Maestro (Schrödinger, LLC). The atomic coordinates and structure factors have been deposited in the Protein Data Bank under the accession codes 6CGL (pH 4.0 crystals), 6CGM (pH 7.0 crystals), and 6CGN (dAMP-soaked pH 7.0 crystals).

b. The structure of the holo-BsR1 dimer at pH 4. Crystals of recombinant and tagless holo-*Bs*R1 (8 mg/mL, 50 mM HEPES pH 7.6, 50 mM NaCl, 5 mM $MgCl_2$, 5 mM DTT, 1% (w/v) glycerol) were obtained anaerobically in a glove box (Coy Laboratory Products) using the sitting-drop vapor diffusion method. Crystals formed in a solution of 0.1 M citric acid (pH 4.0), 1.6 M $(NH_4)_2SO_4$ using a 1:1 ratio of protein solution and crystallization well solution. The crystals were soaked in the well solution supplemented with 15 – 24% ethylene glycol prior to mounting on rayon loops and flash-freezing by direct plunge into liquid nitrogen. A diffraction dataset obtained from a crystal harvested from the initial sparse-matrix screen (Qiagen) was used for structure solution and model building. The crystals contain two molecules of NrdE in the asymmetric unit (ASU), designated as chains A and B. The two molecules in the ASU do not form a physiologically relevant dimer interface. However, a new dimer interface exists between the N-terminus of one monomer with a symmetry-related monomer in the neighboring ASU. Initial refinement of the

dataset with the molecular replacement search model yielded significant unmodeled electron density at this interface consistent with the shape of dAMP. The final model for the holo-BsR1 dimer includes residues 3-162, 166-214, 222-238, and 244-689 for chain A; 3-162, 166-213, 221-238, and 244-687 for chain B; 2 molecules of dAMP; 5 sulfate ions; and 19 water molecules. Short regions of the connector domain (residues 163-165), the specificity site loop (residues 215-220), and a third loop (residues 239-243) connecting the alpha helices at the dimer interface to the catalytic core were disordered.

c. The structure of apo-BsR1 at pH 7. A second crystallization condition at physiological pH (0.1 M HEPES (pH 7.0), 10% (*w*/*v*) PEG 6000) was identified and optimized by addition of 9 mM TCEP to the primary condition. Square-shaped crystals appeared within six weeks in hanging drop vapor diffusion trays and were harvested after cryoprotection in well solution supplemented with 15 – 24% ethylene glycol prior to mounting on rayon loops and flash-freezing by direct plunge into liquid nitrogen. The final model contains one molecule of NrdE in the ASU but two symmetry-related molecules approach the dAMP binding site via disordered loops. These interactions appear to destabilize the ligand binding site, resulting in loss of electron density for dAMP, and the two primary nucleotide anchoring residues in the N-terminal domain (R90 and F37) adopt alternative conformations in this structure. We therefore assigned the structure as apo-NrdE. The final model included residues 6-162, 166-194, 197-214, 222-234, 245-270, and 275-688 for the NrdE polypeptide; 3 ethylene glycol molecules, and 325 water molecules.

d. The structure of holo-BsR1 (dAMP-soaked) at pH 7. The crystal structure of holo-NrdE at pH 7 was obtained by soaking the apo crystals with a freshly-prepared solution of 10 mM dAMP in well solution (100 mM HEPES (pH 7.0), 15 % (*w*/*v*) PEG 6000, 15 mM $MgCl_2$, 1 mM DTT, 15 % (*v*/*v*) ethylene glycol). Crystals were transferred to the soak solution and allowed to equilibrate

for 5-10 min prior to flash-freezing. The best diffraction was achieved with short (<20 min) soaks and the resulting crystals retained the original lattice symmetry and packing. The final model for the dAMP-BsR1 monomer included residues 6-235 and 245-688 for the polypeptide, 1 molecule of dAMP, 1 phosphate ion, 3 ethylene glycol molecules, and 111 water molecules. Many of the previously disordered loops from symmetry mates around the dAMP binding site become ordered in response to addition of the dAMP molecule. The ligand can be modeled at full occupancy in the site observed in the previous structure solved at lower pH. Density for an additional phosphate ion, distinct from the terminal phosphate of the dAMP molecule, is found at an adjacent site. Phosphate is not a component of the crystallization solution or protein storage buffer but could have been introduced as a contaminant from the dAMP stock solution, providing a rationale for its appearance in the soak experiment. This feature of the structure is consistent with the observation that as-isolated holo-NrdE emerges from the cell with small amounts of nucleoside di- and triphosphates bound in addition to the primary monophosphate ligand.

Small-angle X-ray scattering (SAXS). X-ray scattering experiments were performed at the Cornell High Energy Synchrotron Source (CHESS) G1 station on four different occasions using a 250 μm square X-ray beam with an energy of 9.8 or 9.9 keV and flux of $\sim 10^{12}$ photons s^{-1} mm^{-2} at the sample position. Small-angle and wide-angle X-ray scattering (SAXS/WAXS) images were collected simultaneously on two Pilatus 100K photon-counting detectors, covering a range of $q \approx 0.01 - 0.7$ Å^{-1}. q is the momentum transfer variable and is defined as $q = 4\pi/\lambda \sin\theta$, where λ is the X-ray wavelength and θ is the scattering angle. Data processing and analysis were performed using custom code written in MATLAB (The MathWorks, Inc. Natick, MA), BioXTAS RAW (31), and ATSAS (32). The scattering images were integrated about the beam center and normalized by the transmitted intensities measured on a photodiode beamstop as previously

described (33, 34). Background scattering was subtracted from the protein solution scattering to produce the integrated protein scattering profile, $I(q)$, as a function of q. Radii of gyration (R_g) were estimated with Guinier analysis, and the pair distance distribution analysis was performed in GNOM (35).

a. Nucleotide titrations. Titration data were collected on samples of apo-NrdE (2 μM) or holo-NrdE (1 μM) in 50 mM HEPES (pH 7.6), 150 mM NaCl, 15 mM $MgCl_2$, 1 mM TCEP, and 1% (w/v) glycerol with 1 mM CDP and variable concentrations of dAMP or dATP. Background subtraction was performed with carefully matched buffer solutions containing identical concentrations of nucleotides as described previously (34, 36). Samples were prepared fresh and centrifuged at 14,000 x g at 4 °C for 10 min immediately before loading into an in-vacuum flow cell kept at 4 ˚C. For each protein and buffer solution, 20 x 2-s or 40 x 2-s exposures were taken with sample oscillation to limit radiation damage. Singular value decomposition (SVD) was performed in MATLAB.

b. Anion exchange SAXS. Anion exchange (AEX) chromatography-coupled SAXS was performed with a Mono Q GL 5/50 column (GE) operated by a GE Akta Purifier at 4 ˚C with the elution flowing directly into an in-vacuum X-ray sample cell. 500 μL of 15 μM as-isolated NrdE in 50 mM HEPES (pH 7.6), 150 mM NaCl, 15 mM $MgCl_2$, 1 mM TCEP, and 1% (v/v) glycerol was loaded onto the column that was pre-equilibrated in 50 mM Tris, pH 7.6, 100 mM NaCl, 1 mM TCEP, and 1% (w/v) glycerol. The column was washed with 2 column volumes of equilibration buffer and then developed with a linear gradient of 100 - 500 mM NaCl (in 50 mM HEPES (pH 7.6), 15 mM $MgCl_2$, 1 mM TCEP, 1% (w/v) glycerol) over 20 mL at a flow rate of 0.25 mL min^{-1}. 1737 2-s exposures were collected continuously over the course of the elution.

c. Decomposition of scattering curves and elution peaks. AEX-SAXS data were decomposed into four scattering components: two components represented the changing background due to the NaCl gradient, possibly including its effect on the X-ray window, and two components represented eluting protein species (**Figure S9**). The decomposition was performed in MATLAB using the alternating least-squares algorithm (37), modified to include smoothness regularization (38) applied to the elution peaks. Each component's regularization parameter was chosen manually.

d. Structural analysis. Experimental scattering curves were fitted to theoretical scattering profiles of structural models over the q-range 0.008 – 0.7 $Å^{-1}$ using CRYSOL (39). The $\sqrt{\chi^2}$ values were those reported by CRYSOL. To account for scattering from unmodeled residues in the crystal structure of dAMP-loaded NrdE, a homology model of the *B. subtilis* monomer was made in Phyre (40). Models of the non-canonical and canonical dimers were then constructed by aligning the Phyre model of the monomer with the dAMP-bound crystal structure reported here and the previously reported *S. typhimurium* NrdE structure (PDB accession code 1PEQ) (24).

Table S1. Steady-state kinetic parameters for *B. subtilis* RNR measured by the spectrophotometric assay.[a]

S	E[b]	[S] range (μM)	V_{max} (U mg^{-1} $\alpha_2\beta_2$)	k_{cat} (s^{-1})	K_m (μM)	k_{cat} K_m^{-1} (x10^3 M^{-1} s^{-1})	n_H
ADP	dGTP	25 - 8000	570 ± 20	2.30 ± 0.10	490 ± 80[c]	4.8 ± 0.8	0.7 ± 0.1
GDP	TTP	10 - 1000	200 ± 5	0.80 ± 0.02	25 ± 2[c]	33 ± 3.0	1.8 ± 0.3
CDP	ATP	10 – 2000	310 ± 9	1.30 ± 0.04	71 ± 9	17 ± 2.0	1
CDP	dATP	25 – 2000	260 ± 6	1.10 ± 0.02	150 ± 10	7.1 ± 0.5	1
UDP	ATP	25 – 4000	400 ± 10	1.70 ± 0.05	160 ± 20	11 ± 1.0	1
UDP	dATP	25 – 3000	270 ± 5	1.10 ± 0.02	160 ± 10	6.8 ± 0.6	1

[a] Assay conditions: 37 °C, 0.5 μM His_6-Mnβ_2, 0.5 μM His_6-α_2 (aiNrdE), 0.2 mM NADPH, 40 μM TrxA, 0.4 μM TrxB, 50 mM HEPES, pH 7.6, 15 mM $MgCl_2$, 1 mM EDTA.

[b] Effector concentrations were held at ~10x their apparent K_m (ATP = 2.9 mM, dGTP = 20 μM, TTP = 15 μM) or, for dATP, those that gave maximum activity (2.5 μM and 5 μM for CDP and UDP, respectively).

[c] These values are K_m^{app} as the data were fit with the Hill equation.

Table S2. Apparent steady-state affinity of *B. subtilis* RNR for effector nucleotides measured by the spectrophotometric assay.[a]

E	S	[E] range (μM)	K_m (μM)
ATP	CDP	50 – 4000	200 ± 30
ATP	UDP	25 – 4000	350 ± 40
dGTP	ADP	0.25 - 4000	1.7 ± 0.2
TTP	GDP	0.10 – 4000	1.2 ± 0.1

[a] Assay conditions: 37 °C, 0.5 μM His_6-Mnβ_2, 0.5 μM His_6-α_2 (aiNrdE), 0.2 mM NADPH, 40 μM TrxA, 0.4 μM TrxB, 50 mM HEPES, pH 7.6, 15 mM $MgCl_2$, 1 mM EDTA. Substrate concentrations were held at 1 mM.

Table S3. X-ray crystallography data collection and refinement statistics.

	Holo-*Bs*NrdE (pH 4.0)	Apo-*Bs*NrdE (pH 7.0)	dAMP-soaked apo-*Bs*NrdE (pH 7.0)
PDB accession code	6CGL	6CGM	6CGN
Data collection			
Space group	*C* 2 2 2_1	*P* 4_3 2_1 2	*P* 4_3 2_1 2
Cell dimensions			
a, *b*, *c* (Å)	161.6, 182.1, 155.3	72.86, 72.86, 296.14	72.27, 72.27, 292.64
α, β, γ (°)	90.0, 90.0, 90.0	90.0, 90.0, 90.0	90.0, 90.0, 90.0
Resolution (Å)*	50.0-3.20 (3.26-3.20)	50.0-2.00 (2.03-2.00)	48.24-2.26 (2.30-2.26)
R_{merge}	0.224 (0.724)	0.114 (0.778)	0.188 (1.915)
R_{pim}	0.092 (0.328)	0.024 (0.237)	0.050 (0.506)
$I / \sigma I$	8.0 (2.0)	36.5 (3.0)	16.75 (2.0)
$CC_{1/2}$	0.916	0.827	0.772
Completeness (%)	93.5 (71.8)	99.5 (97.9)	99.8 (98.7)
Redundancy	5.7 (4.3)	20.9 (10.4)	14.0 (14.2)
Refinement			
Resolution (Å)	120.88-3.20	74.0-2.00	73.16-2.26
No. reflections	35620	55007	37497
R_{work} / R_{free}	0.197/0.252	0.193/0.235	0.220/0.246
No. atoms	11007	5679	5629
Protein	10919	5342	5479
Ligand/ion	44	0	27
Water/solvent	44	337	123
B-factors			
Protein	74.99	30.02	35.26
Ligand/ion	103.49	-	28.36
Water/solvent	62.21	31.78	31.72
rms deviations			
Bond lengths (Å)	0.007	0.009	0.0066
Bond angles (°)	1.010	1.310	1.019
Molprobity clash score	1.06 (100^{th} percentile)	1.13 (100^{th} percentile)	0.82 (100^{th} percentile)
Rotamer outliers (%)	0.76	0.69	0.17
Ramachandran favored (%)	95.85	97.83	98.06

*Values in parentheses are for highest-resolution shell.

Table S4. Primers used in this study.

Cloning *B. subtilis* RNR genes into pE-SUMO		
Gene	**Primer direction**	**Sequence**[a]
nrdE	Forward	5′-AGGAGGTCTCAAGGT**ATG**TCACAAAATCAAGTGCCAAAATGG-3′
	Reverse	5′-TCTCGAGC**TCA**AACAACACAAGAAAGGCAGC-3′
nrdI	Forward	5′-AGGTGGTCTCAAGGT**ATG**GTACAAATCATATTTGATTCG-3′
	Reverse	5′-CATGCTCGAG**TTA**TTTAACTGGATCCATTTTGGC-3′
nrdF	Primer#1	5′-AGAGCTCGGTCTCCTTGCTCAGGAAATTTATAATAAACAG-3′
	Primer#2	5′-ATATATCTCGAG**TTA**TATCTGCTCTTTTTCATCTTCAAAA-3′
	Primer#3	5′-ATATATGGTCTCCAGGT**ATG**ACAAAAATTTATGACGCAGC-3′
	Primer#4	5′-CCTGAGCAAGGAGACCGACATACACGCCGTGAATCGC-3′
Site-directed mutagenesis of pE-SUMO-*nrdE*		
Mutant	**Primer direction**	**Sequence**[b]
$H_{34}Q$	Forward	5′-GATAAGGATAAAGAAGCTGTACAGAGCTATTTTGTAG-3′
	Reverse	5′-CTACAAAATAGCTCTGTACAGCTTCTTTATCCTTATC-3′
$F_{37}I$	Forward	5′-GCTGTACATAGCTATATTGTAGATTATATCAATCAAAAC-3′
	Reverse	5′-GTTTTGATTGATATAATCTACAATATAGCTATGTACAGC-3′

[a] Restriction sites are underlined, and start and stop codons are indicated in boldface font.
[b] Mutated codons are underlined.

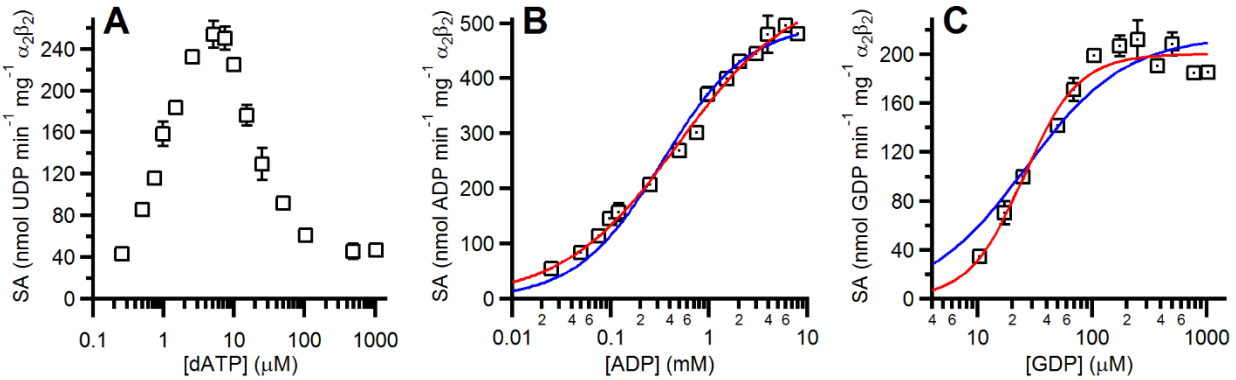

Figure S1. Kinetic analyses of *B. subtilis* Ib RNR. Spectrophotometric assays were conducted at 37 °C in 500 μL using a 1:1 ratio of His_6-tagged subunits (0.5 μM each; aiNrdE), the endogenous reducing system, and the substrate and effector nucleotides indicated. (**A**) The inhibitory effects of dATP on the reduction of UDP (held at 1 mM). The right two panels show the comparison of the fits to the Michaelis-Menten (blue) and Hill (red) equations for the steady-state kinetic data with (**B**) ADP as the variable substrate ([dGTP] = 20 μM), and (**C**) GDP as the variable substrate ([TTP] = 15 μM). Fits of the data to the Hill equation are statistically better than to the Michaelis-Menten equation based on a nested model F-ratio test using a threshold $p = 0.01$ ($p = 0.0003$ in **B** and 0.002 in **C**). The data are the average of three measurements, and in many cases the error bars (± 1 SD) are smaller than the marker size.

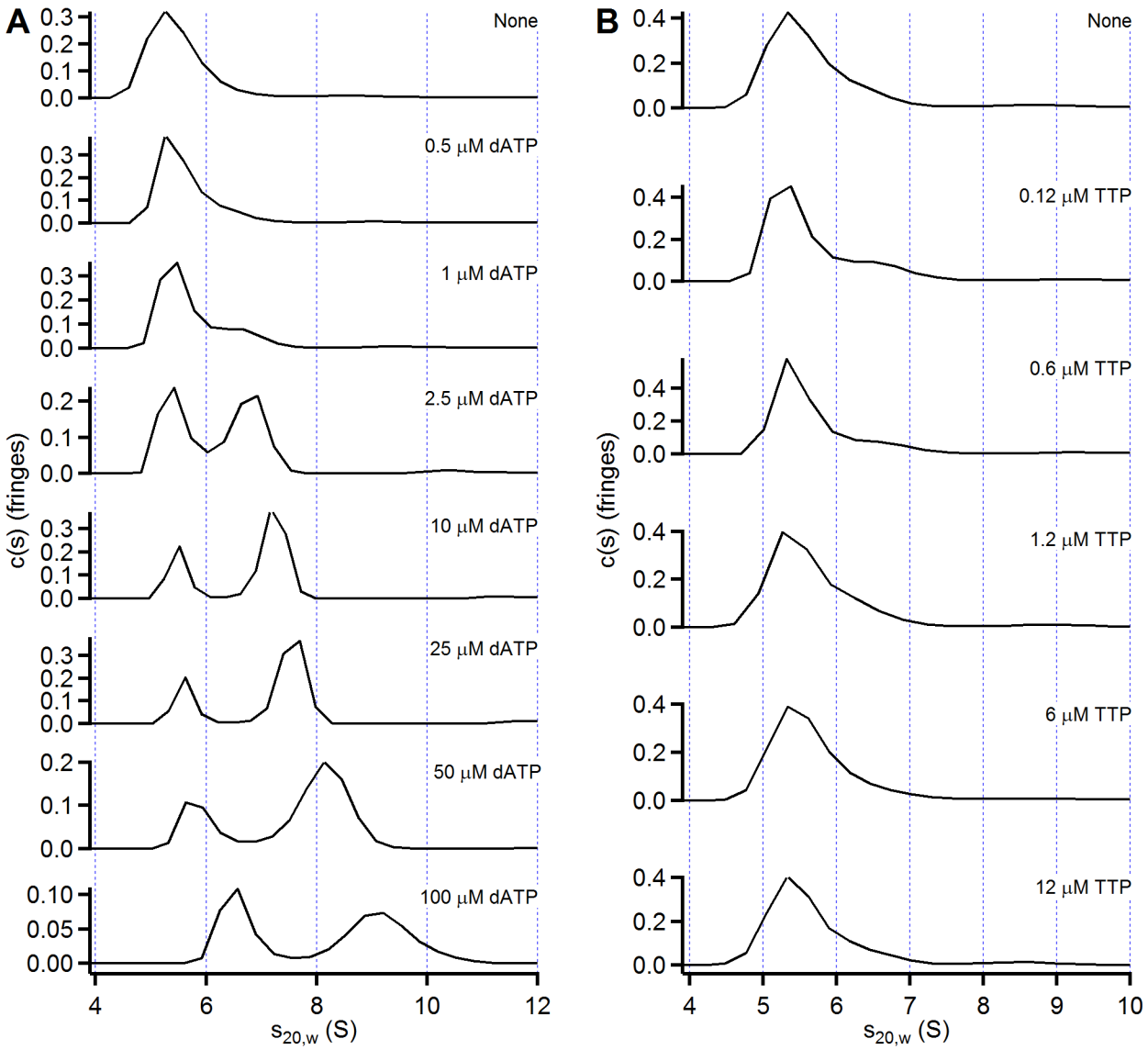

Figure S2. SV-AUC analysis of recombinant *B. subtilis* aiNrdE in the presence of nucleotides. (**A**) $s_{20,w}$ distributions for 1.0 μM aiNrdE in the presence of dATP at the concentrations indicated in the upper right corner of each graph. For detailed description of analysis at 100 μM dATP, refer to methods. (**B**) $s_{20,w}$ distributions for 1.2 μM aiNrdE in the presence of the indicated concentrations of TTP.

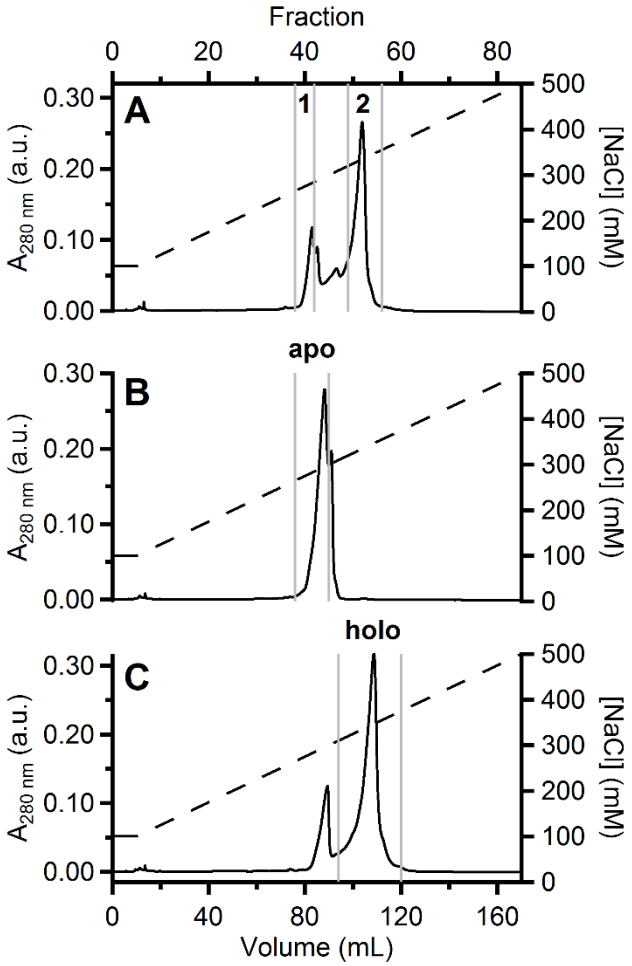

Figure S3. Separation of holo- and apo-NrdE by anion exchange chromatography on a MonoQ column. The solid line is the A_{280} and the dashed line the NaCl gradient. Note that all experiments were performed with the same gradient. Vertical grey bars indicate the limits of fraction pooling for each separation. (**A**) Separation of aiNrdE. **1,** apo-NrdE fraction pool; **2,** holo-NrdE fraction pool. (**B**) Second round of chromatography for an apo-NrdE sample from **1** pooled from multiple fractionations of aiNrdE. (**C**) Second round of chromatography for a holo-NrdE sample from **2** pooled from multiple fractionations of aiNrdE.

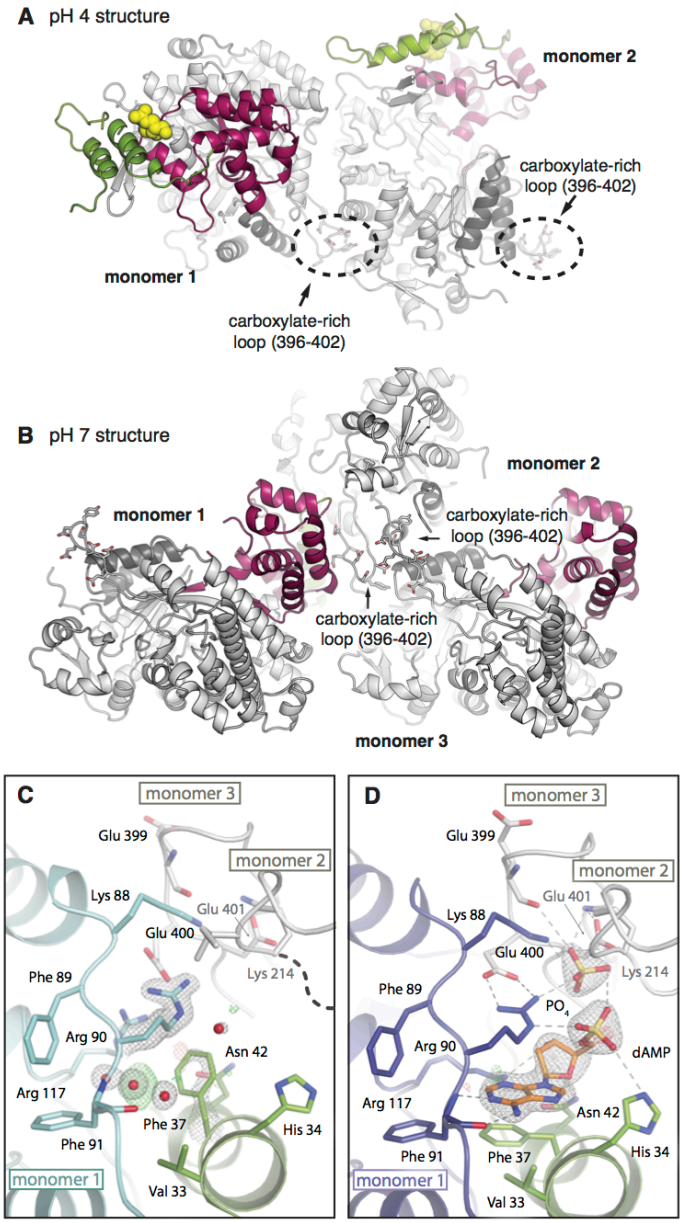

Figure S4. A view of the crystal packing interactions in the (**A**) pH 4 *Bs* NrdE holoenzyme structure and (**B**) pH 7 *Bs* NrdE apo structure. Zoomed-in views of the lattice contacts with symmetry mates in the (**C**) pH 7 apo and (**D**) dAMP-soaked structures. $2F_o$-F_c electron density map (2.0 σ, grey mesh) and F_o-F_c difference map (3.0 σ, green mesh) are shown for selected side chains and ligands. Our analysis of these structures suggests that the occurrence of a carboxylate-rich loop in the α subunit, a feature that is specific to the *B. subtilis* system and a few closely related enzymes, appears to encourage non-native ionic interactions between monomers at the high concentrations of enzyme present in the crystal lattice. This phenomenon would be altered at increased pH and provides an explanation for disruption of the binding pocket by the lattice-induced (and non-physiologically-relevant) contacts that seemingly result in loss of the dAMP monomer in the crystal at pH 7.

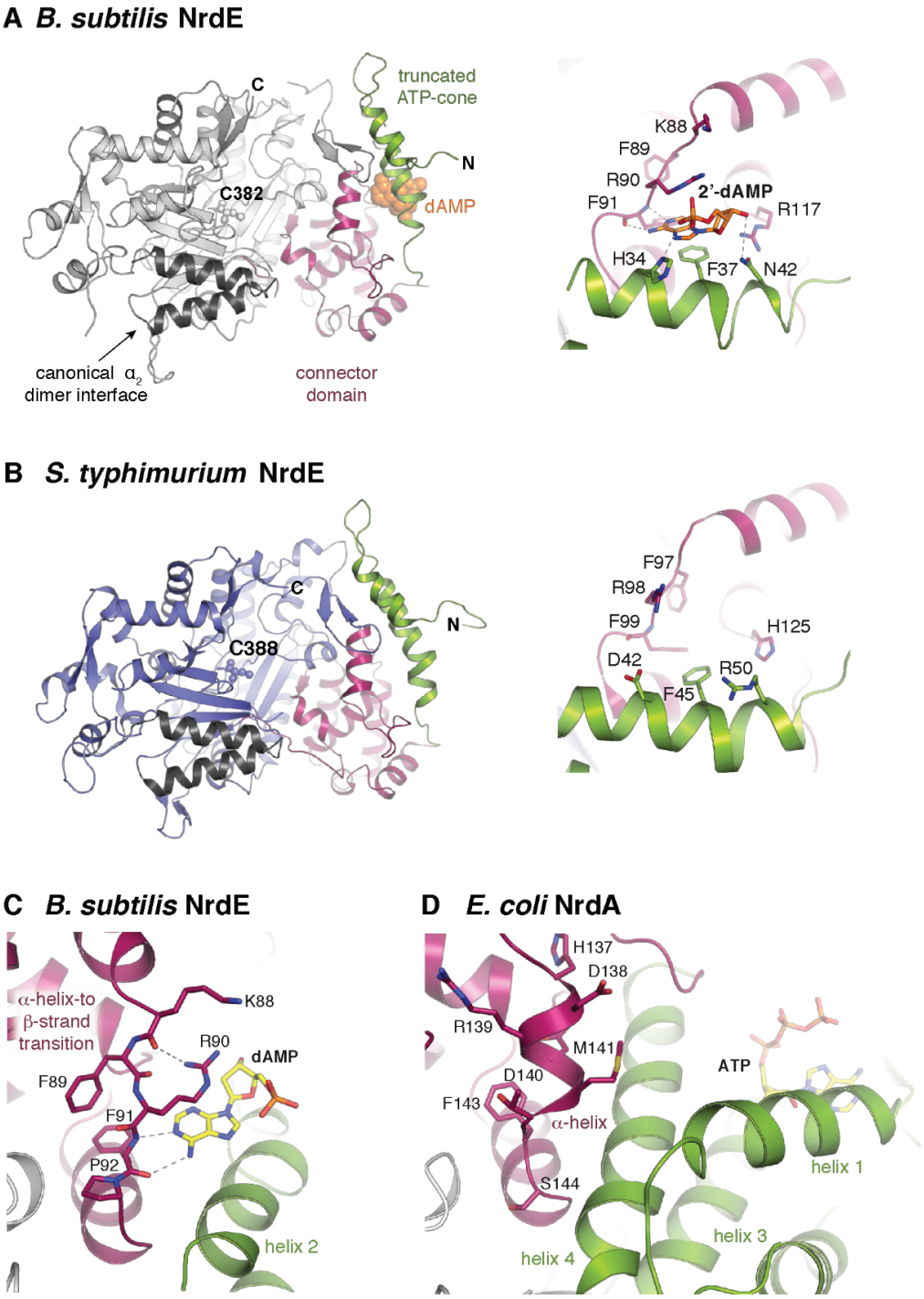

Figure S5. Structural conservation of the N-terminal nucleotide binding sites in class Ib and Ia RNRs. A comparison of (**A**) the *Bs* NrdE and (**B**) *St* NrdE (PDB: 1PEM) reveals conservation of residues lining the dAMP binding site. (**C**) In *Bs* NrdE, the dAMP binding site involves a reverse adenine-binding motif in the connector domain. (**D**) In the class Ia NrdA from *E. coli* (PDB: 3R1R), the connector domain in the vicinity of the nucleotide-binding site is more α-helical and packs more tightly against the last helix in the ATP-cone structure.

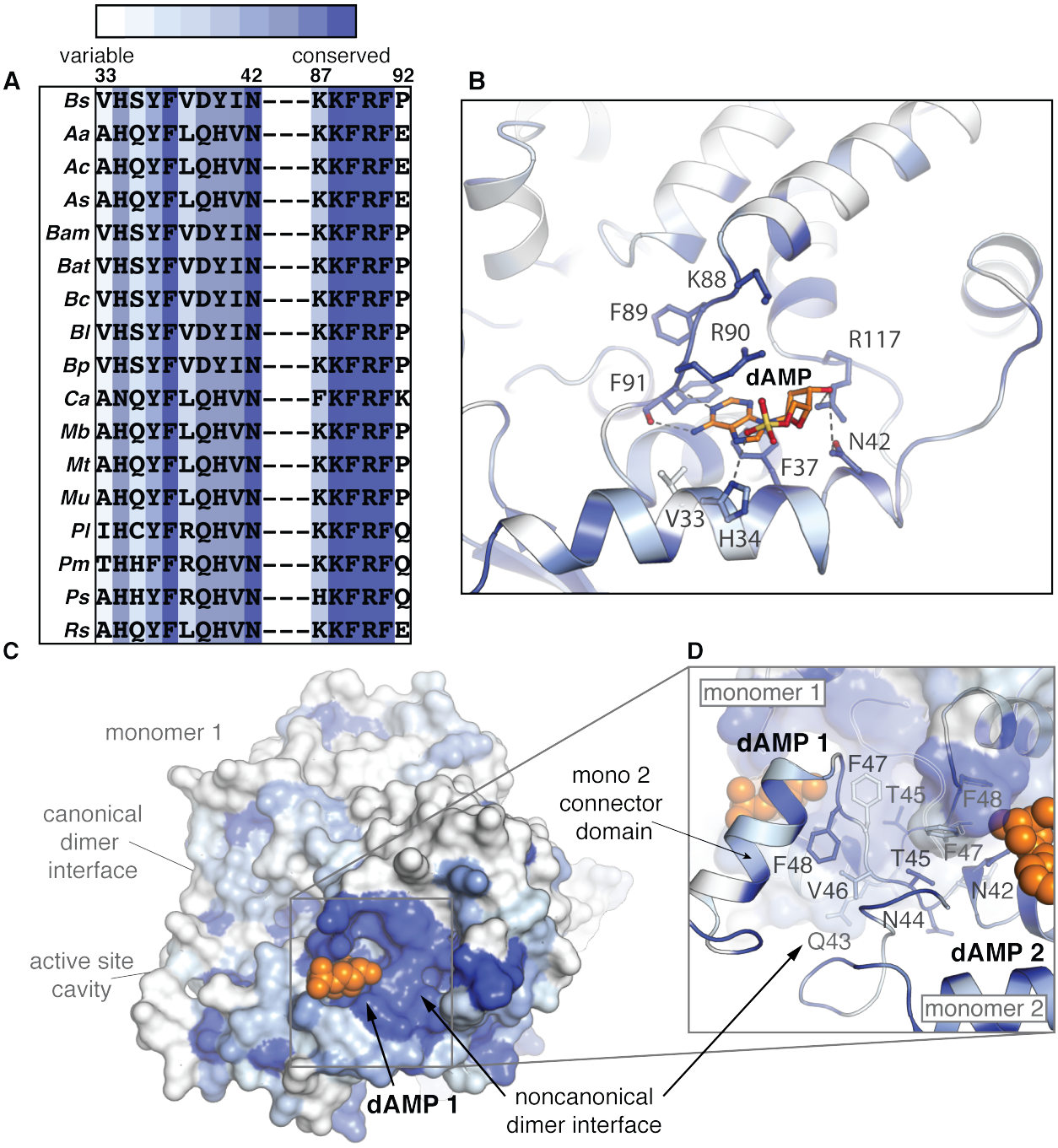

Figure S6. Sequence conservation of the dAMP binding site in selected class Ib NrdE homologs predicted to undergo dAMP-mediated activity modulation. (**A**) Sequence alignment of homologs in regions near the dAMP binding site in *Bs* NrdE. *Aa* = *Arthrobacter aurescens* TC1, *Ac* = *Arthrobacter chlorophenolicus* A6, *As* = *Arthrobacter species* FB24, *Bam* = *Bacillus amyloliquefaciens* FZB42, *Bat* = *Bacillus atrophaeus* 1492, *Bc* = *Bacillus clausii* KSMK16, *Bl* = *Bacillus licheniformis* 14580, *Bp* = *Bacillus pumilus* 7061, *Ca* = *Corynebacterium ammoniagenes, Mb* = *Mycobacterium bovis* AF2122/97, *Mt* = *Mycobacterium tuberculosis* H37Rv, *Mu* = *Mycobacterium ulcerans* Agy99, *Pl* = *Photorhabdus mirabilis* HI4320, *Pm* = *Proteus mirabilis*

HI4320, *Ps = Providencia stuartii* 25827, *Rs = Renibacterium salmoninarum* 33209. Color scale indicates degree of sequence conservation (white is variable and blue is conserved). (**B**) In the selected subset of class Ib RNRs, a ConSurf (41) analysis (http://consurf.tau.ac.il) shows that the NrdE residues that directly interact with dAMP are similar within this group. (**C**, **D**) Analysis of the molecular surface around the dAMP binding pocket and at the non-canonical dimer interface shows that these regions are also highly conserved in this subset of class Ib RNRs. Selected side chains are shown in stick format and dAMP is shown as a space-filling model (orange).

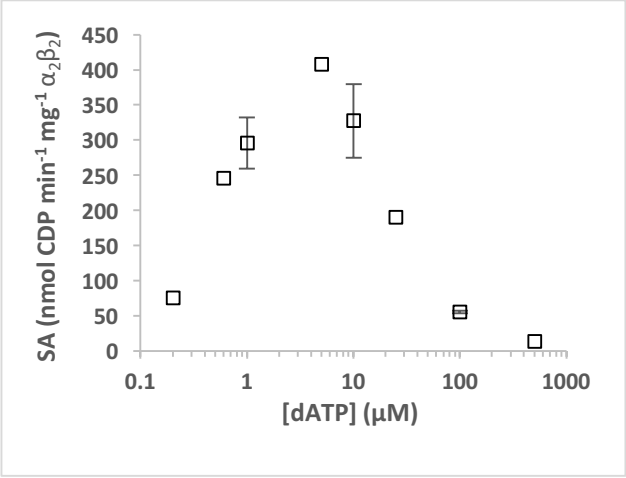

Figure S7. H34Q NrdE displays a similar dATP inhibition profile as apo-NrdE (main text Fig. 3). Following MonoQ AEX, the final H34Q NrdE fraction was concentrated to 30 μM monomer (in 50 mM Tris pH 7.6, 5 % glycerol, ~290 mM NaCl, 1 mM TCEP). Spectrophotometric assays (500 μL) were conducted at 37 °C using 1 mM CDP, the indicated concentrations of dATP, the endogenous reducing system (40 μM TrxA, 0.4 μM TrxB, 0.2 mM NADPH), and a 1:1 ratio of $Mn(III)_2$-Y▪ NrdF and NrdE H34Q (0.5 μM each).

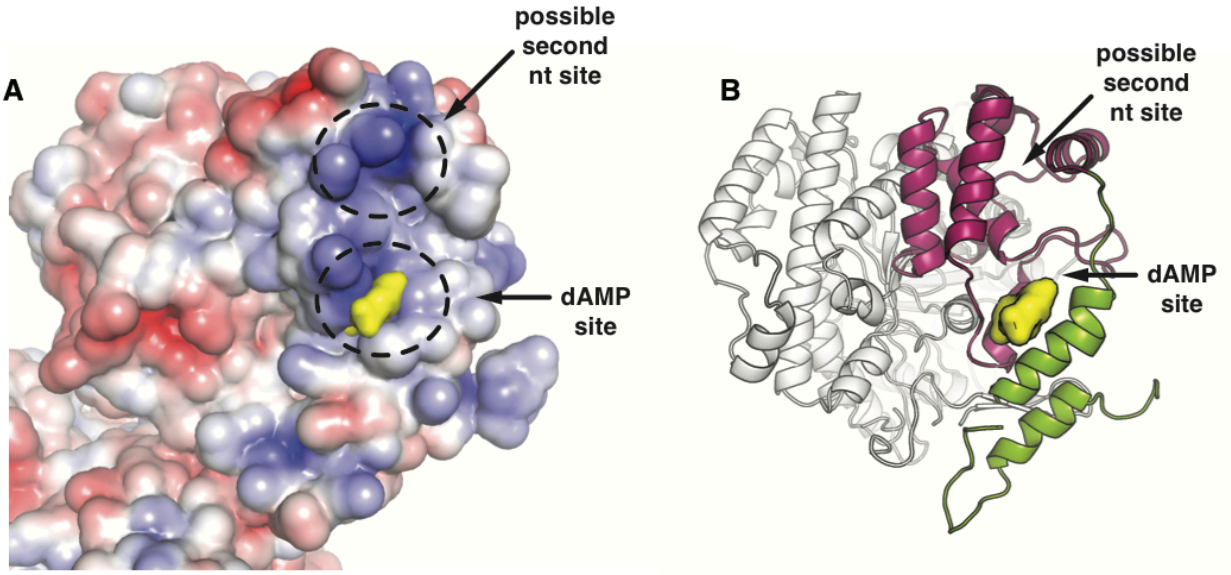

Figure S8. (**A**) An electrostatic surface potential map (red -5 k_BT, blue +5 k_BT) (42) of the N-terminal domain in *Bs* NrdE shows the possible nucleotide-binding pockets in this region of the protein. (**B**) A cartoon diagram of the domain architecture is shown in the same orientation for reference. The dAMP ligand is shown as a yellow surface.

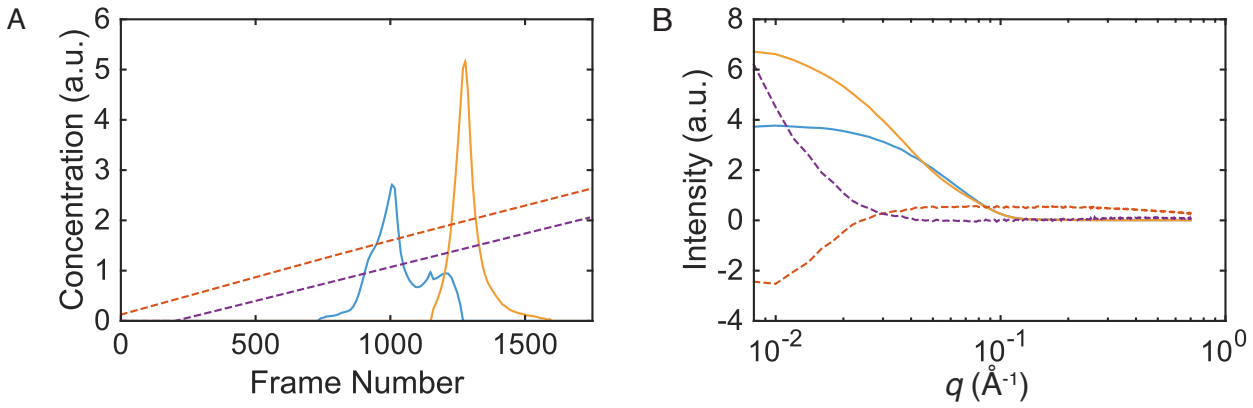

Figure S9. Four-component decomposition of the NrdE AEX-SAXS dataset. (**A**) Elution peaks for the two protein components (blue, orange) and sloping background components due to the NaCl gradient (dashed lines). (**B**) SAXS profiles corresponding to each elution peak.

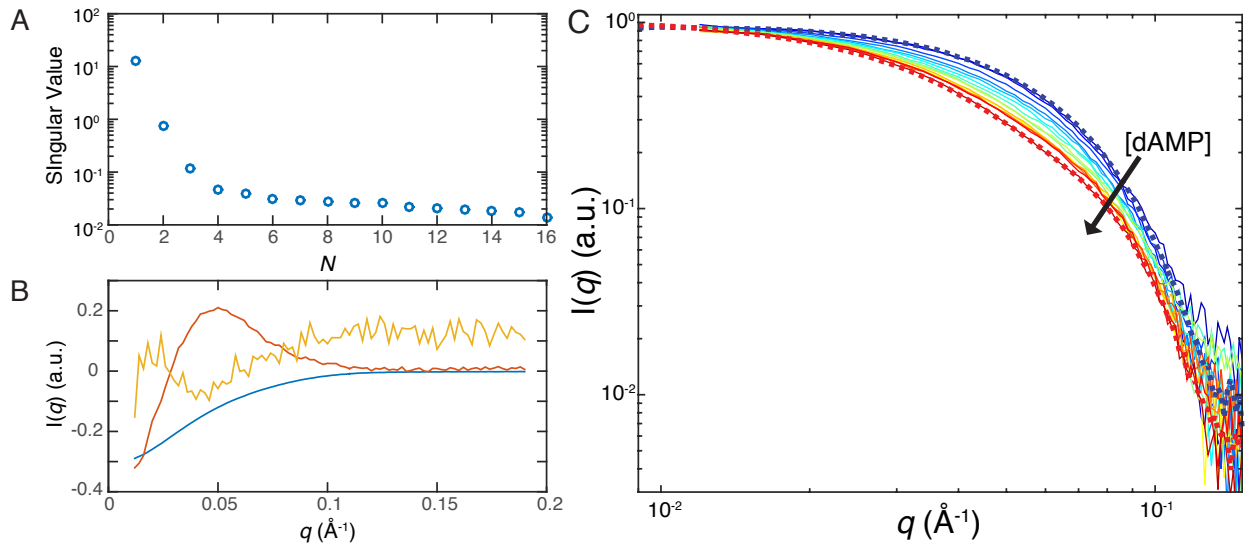

Figure S10. Titration of 0-300 μM dAMP induces a transition from apo- to holo-NrdE. (**A**) SVD of the dAMP titration dataset yields two major singular values. (**B**) The first two singular vectors (blue, red) account for the bulk of the change in scattering. A third singular vector accounts (orange) for errors in background subtraction. (**C**) Scattering profiles of dAMP titration (solid lines, blue to red) overlaid with the scattering of the AEX-derived monomer (blue dashed) and non-canonical dimer (red dashed).

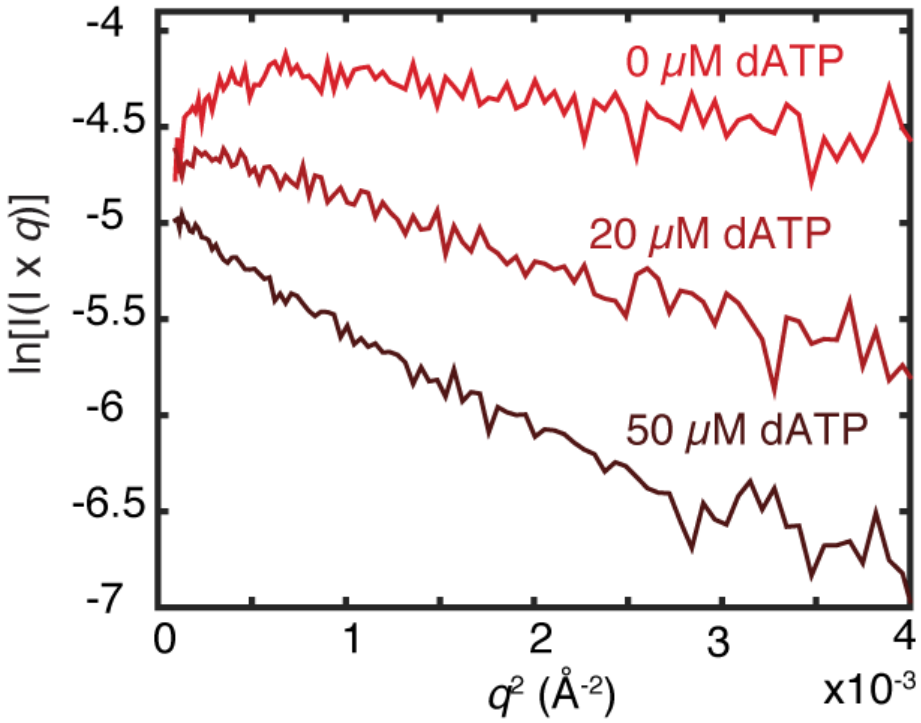

Figure S11. The scattering curves from 1 μM NrdE + 0 – 50 μM dATP (same data shown in Fig. 7E of the main text) are plotted here as cross-sectional Guinier plots: ln(I x q) vs q^2 . The low q region becomes increasingly linear with the addition of dATP, indicative of the formation of an elongated species.

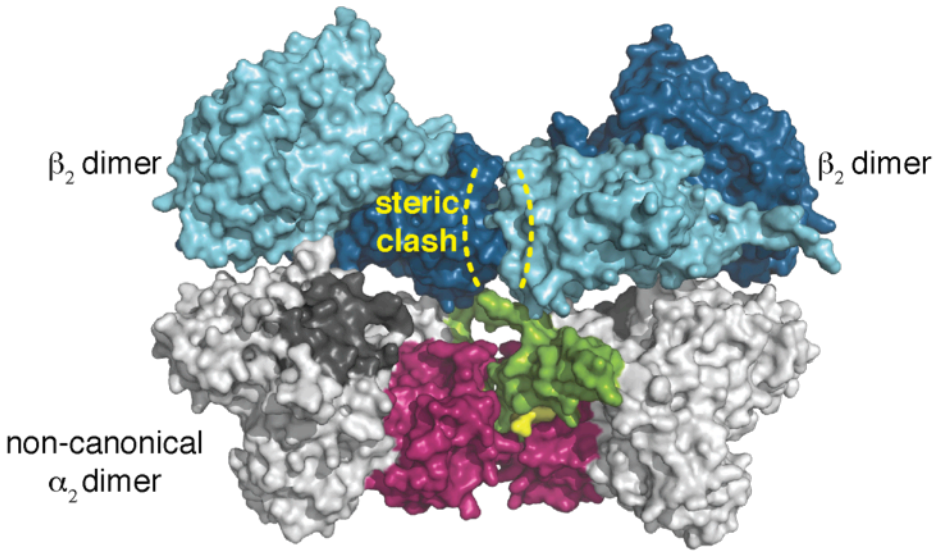

Figure S12. A docking model (43) of holoenzyme assembly starting from the non-canonical dAMP-bound α_2 dimer exhibits steric clash between adjacent β_2 dimers. Partial ATP-cone shown in green, N-terminal connector domain shown in magenta, and catalytic core shown in gray. The helices of the canonical α_2 dimer interface are shown in dark gray and dAMP is shown as a yellow space-filling model. The β monomers are shown in light and dark blue.

Supporting References

1. Parker MJ (2017) Discovery and Investigation of the Novel Overall Activity Allosteric Regulation of the *Bacillus subtilis* Class Ib Ribonucleotide Reductase. Ph.D. Thesis (Massachusetts Institute of Technology, Cambridge, MA).
2. Korbie DJ & Mattick JS (2008) Touchdown PCR for Increased Specificity and Sensitivity in PCR Amplification. *Nat. Protoc.* 3(9):1452-1456.
3. Cotruvo JA, Stich TA, Britt RD, & Stubbe J (2013) Mechanism of Assembly of the Dimanganese-Tyrosyl Radical Cofactor of Class Ib Ribonucleotide Reductase: Enzymatic Generation of Superoxide Is Required for Tyrosine Oxidation via a Mn(III)Mn(IV) Intermediate. *J. Am. Chem. Soc.* 135(10):4027-4039.
4. Parker MJ, Zhu X, & Stubbe J (2014) *Bacillus subtilis* Class Ib Ribonucleotide Reductase: High Activity and Dynamic Subunit Interactions. *Biochemistry* 53(4):766-776.
5. Zhang Y & Stubbe J (2011) *Bacillus subtilis* Class Ib Ribonucleotide Reductase is a Dimanganese(III)-Tyrosyl Radical Enzyme. *Biochemistry* 50(25):5615-5623.
6. Gasteiger E*, et al.* (2005) Protein Identification and Analysis Tools on the ExPASy Server. *The Proteomics Protocols Handbook*, ed Walker JM (Humana Press, Totowa, NJ), pp 571-607.
7. Smith PK*, et al.* (1985) Measurement of Protein Using Bicinchoninic Acid. *Anal. Biochem.* 150(1):76-85.
8. Mayhew SG & Massey V (1969) Purification and Characterization of Flavodoxin from *Peptostreptococcus elsdenii*. *J. Biol. Chem.* 244(4):794-802.
9. Edelhoch H (1967) Spectroscopic Determination of Tryptophan and Tyrosine in Proteins. *Biochemistry* 6(7):1948-1954.
10. Gill SC & von Hippel PH (1989) Calculation of Protein Extinction Coefficients from Amino Acid Sequence Data. *Anal. Biochem.* 182(2):319-326.
11. Zhao HY*, et al.* (2013) Recorded Scan Times can Limit the Accuracy of Sedimentation Coefficients in Analytical Ultracentrifugation. *Anal. Biochem.* 437(1):104-108.
12. Zhao HY*, et al.* (2010) Accounting for Solvent Signal Offsets in the Analysis of Interferometric Sedimentation Velocity Data. *Macromol. Biosci.* 10(7):736-745.
13. Balbo A & Schuck P (2005) Analytical Ultracentrifugation in the Study of Protein Self-Association and Heterogeneous Protein-Protein Interactions. *Protein-Protein Interactions: A Molecular Cloning Manual*, eds Golemis EA & Adams PD (Cold Spring Harbor Laboratory Press, New York), pp 253-277.
14. Schuck P (2003) On the Analysis of Protein Self-Association by Sedimentation Velocity Analytical Ultracentrifugation. *Anal. Biochem.* 320(1):104-124.
15. Laue TM, Shah BD, Ridgeway TM, & Pelletier SL (1992) Computer-Aided Interpretation of Analytical Sedimentation Data for Proteins. *Analytical Ultracentrifugation in Biochemistry and Polymer Science*, eds Harding SE, Rowe AJ, & Horton JC (Royal Society of Chemistry, Cambridge), pp 90-125.
16. Ortega A, Amorós D, & de la Torre JG (2011) Prediction of Hydrodynamic and Other Solution Properties of Rigid Proteins from Atomic- and Residue-Level Models. *Biophys. J.* 101(4):892-898.
17. Philo JS (2006) Improved Methods for Fitting Sedimentation Coefficient Distributions Derived by Time-Derivative Techniques. *Anal. Biochem.* 354(2):238-246.

18. Stafford WF, III (1992) Boundary Analysis in Sedimentation Transport Experiments: A Procedure for Obtaining Sedimentaiton Coefficient Distributions Using the Time Derivative of the Concentration Profile. *Anal. Biochem.* 203(2):295-301.
19. Randerath K & Randerath E (1964) Ion-Exchange Chromatography of Nucleotides on Poly-(Ethyleneimine)-Cellulose Thin Layers. *J. Chromatogr. A* 16(1):111-125.
20. Rowley GL & Kenyon GL (1974) PEI-Cellulose Thin-Layer Chromatography - Product Studies of Creatine Kinase and Pyruvate Kinase Reactions. *Anal. Biochem.* 58(2):525-533.
21. Otwinowski Z & Minor W (1997) Processing of X-ray Diffraction Data Collected in Oscillation Mode. *Methods Enzymol.* 276:307-326.
22. Karplus PA & Diederichs K (2012) Linking Crystallographic Model and Data Quality. *Science* 336(6084):1030-1033.
23. Long F, Vagin AA, Young P, & Murshudov GN (2008) BALBES: A Molecular-Replacement Pipeline. *Acta Crystallogr. Sect. D-Biol. Crystallogr.* 64:125-132.
24. Uppsten M*, et al.* (2003) Structure of the Large Subunit of Class Ib Ribonucleotide Reductase from *Salmonella typhimurium* and Its Complexes with Allosteric Effectors. *J. Mol. Biol.* 330(1):87-97.
25. Murshudov GN, Vagin AA, & Dodson EJ (1997) Refinement of Macromolecular Structures by the Maximum-Likelihood Method. *Acta Crystallogr. Sect. D-Biol. Crystallogr.* 53:240-255.
26. Winn MD*, et al.* (2011) Overview of the CCP4 Suite and Current Developments. *Acta Crystallogr. Sect. D-Biol. Crystallogr.* 67:235-242.
27. Emsley P & Cowtan K (2004) Coot: Model-Building Tools for Molecular Graphics. *Acta Crystallogr. Sect. D-Biol. Crystallogr.* 60:2126-2132.
28. Chen VB*, et al.* (2010) MolProbity: All-Atom Structure Validation for Macromolecular Crystallography. *Acta Crystallogr. Sect. D-Biol. Crystallogr.* 66:12-21.
29. Ten Eyck LF (1985) Fast Fourier-Transform Calculation of Electron-Density Maps. *Methods Enzymol.* 115:324-337.
30. Ashkenazy H*, et al.* (2016) ConSurf 2016: An Improved Methodology to Estimate and Visualize Evolutionary Conservation in Macromolecules. *Nucleic Acids Res.* 44(W1):W344-W350.
31. Hopkins JB, Gillilan RE, & Skou S (2017) BioXTAS RAW: Improvements to a Free Open-Source Program for Small-Angle X-ray Scattering Data Reduction and Analysis. *J. Appl. Crystallogr.* 50(5):1545-1553.
32. Franke D*, et al.* (2017) ATSAS 2.8: A Comprehensive Data Analysis Suite for Small-Angle Scattering from Macromolecular Solutions. *J. Appl. Crystallogr.* 50(4):1212-1225.
33. Meisburger SP*, et al.* (2016) Domain Movements upon Activation of Phenylalanine Hydroxylase Characterized by Crystallography and Chromatography-Coupled Small-Angle X-ray Scattering. *J. Am. Chem. Soc.* 138(20):6506-6516.
34. Skou S, Gillilan RE, & Ando N (2014) Synchrotron-Based Small-Angle X-ray Scattering of Proteins in Solution. *Nat. Protoc.* 9:1727.
35. Svergun DI (1992) Determination of the Regularization Parameter in Indirect-Transform Methods Using Perceptual Criteria. *J. Appl. Crystallogr.* 25(4):495-503.
36. Ando N*, et al.* (2016) Allosteric Inhibition of Human Ribonucleotide Reductase by dATP Entails the Stabilization of a Hexamer. *Biochemistry* 55(2):373-381.
37. Maeder M & Neuhold YM (2007) *Practical Data Analysis in Chemistry* (Elsevier, Cambridge) 1st Ed p 340.

38. Press WH, Teukolsky SA, Vetterling WT, & Flannery BP (2007) *Numerical Recipes: The Art of Scientific Computing* (Cambridge University Press, New York) 3rd Ed p 1235.
39. Svergun DI, Barberato C, & Koch MHJ (1995) CRYSOL - A Program to Evaluate X-Ray Solution Scattering of Biological Macromolecules from Atomic Coordinates. *Journal of Applied Crystallography* 28:768-773.
40. Kelley LA, Mezulis S, Yates CM, Wass MN, & Sternberg MJE (2015) The Phyre2 Web Portal for Protein Modeling, Prediction and Analysis. *Nat. Protoc.* 10(6):845-858.
41. Landau M*, et al.* (2005) ConSurf 2005: The Projection of Evolutionary Conservation Scores of Residues on Protein Structures. *Nucleic Acids Res.* 33:W299-W302.
42. Jurrus E *et al.* (2018) Improvements to the APBS Biomolecular Solvation Software Suite. *Protein Sci.* 27: 112-128.
43. Uhlin U & Eklund H (1994) Structure of Ribonucleotide Reductase Protein R1. *Nature* 370(6490):533-539.